ACS APPLIED MATERIALS & INTERFACES

Research Article

www.acsami.org

N-Trimethyl Chitosan Chloride-Coated PLGA Nanoparticles Overcoming Multiple Barriers to Oral Insulin Absorption

Jianyong Sheng,[†] Limei Han,[†] Jing Qin,[†] Ge Ru,[†] Ruixiang Li,[†] Lihong Wu,[‡] Dongqi Cui,[‡] Pei Yang,[†] Yuwei He,[†] and Jianxin Wang*[,†]

[†]Key Laboratory of Smart Drug Delivery, Ministry of Education & PLA, Department of Pharmaceutics, School of Pharmacy, Fudan University, 826 Zhangheng Road, Shanghai 201203, China

[‡]Department of Pharmaceutics, School of Pharmacy, Heilongjiang University of Chinese Medicine, Haerbin, Heilongjiang 150040, China

Supporting Information

ABSTRACT: Although several strategies have been applied for oral insulin delivery to improve insulin bioavailability, little success has been achieved. To overcome multiple barriers to oral insulin absorption simultaneously, insulin-loaded *N*-trimethyl chitosan chloride (TMC)-coated polylactide-*co*-glycoside (PLGA) nanoparticles (Ins TMC-PLGA NPs) were formulated in our study. The Ins TMC-PLGA NPs were prepared using the double-emulsion solvent evaporation method and were characterized to determine their size (247.6 ± 7.2 nm), ζ-potential (45.2 ± 4.6 mV), insulin-loading capacity (7.8 ± 0.5%) and encapsulation efficiency (47.0 ± 2.9%). The stability and insulin release of the nanoparticles in enzyme-containing simulated gastrointestinal fluids suggested that the TMC-PLGA NPs could partially protect insulin from enzymatic degradation. Compared with unmodified PLGA NPs, the positively charged TMC-PLGA NPs could improve the mucus penetration of insulin in mucus-secreting HT29-MTX cells, the cellular uptake of insulin via clathrin- or adsorption-mediated endocytosis in Caco-2 cells and the permeation of insulin across a Caco-2 cell monolayer through tight junction opening. After oral administration in mice, the TMC-PLGA NPs moved more slowly through the gastrointestinal tract compared with unmodified PLGA NPs, indicating the mucoadhesive property of the nanoparticles after TMC coating. Additionally, in pharmacological studies in diabetic rats, orally administered Ins TMC-PLGA NPs produced a stronger hypoglycemic effect, with 2-fold higher relative pharmacological availability compared with unmodified NPs. In conclusion, oral insulin absorption is improved by TMC-PLGA NPs with the multiple absorption barriers overcome simultaneously. TMC-PLGA NPs may be a promising drug delivery system for oral administration of macromolecular therapeutics.

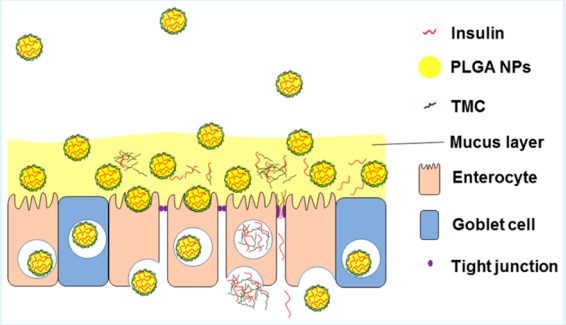

KEYWORDS: *nanoparticles, insulin, oral delivery, N-trimethyl chitosan chloride, absorption barriers, tight junctions, mucus*

1. INTRODUCTION

Insulin is commonly used to treat diabetes.[1] Oral delivery has become the most desirable method of insulin administration because of its convenience and good patient compliance. More importantly, the physiological mechanism of insulin secretion is mimicked by oral administration.[2] In particular, insulin absorbed in the intestine can go directly to the liver, the main target organ of insulin, through the portal vein, and high exposure via the peripheral circulation can be avoided.[3] Consequently, oral delivery of insulin results in fewer side effects. However, the oral bioavailability of protein/peptide therapeutics such as insulin is very poor, mainly due to the following three barriers: (A) Enzyme barrier: insulin is susceptible to digestion by proteases in the gastrointestinal (GI) tract.[4] (B) Mucus barrier: the GI tract is coated with a mucus layer that may prevent macromolecules or drug delivery systems from reaching beneath the epithelial cells.[5,6] (C) Epithelial cell barrier: because of the poor cellular uptake of a hydrophilic macromolecule in epithelial cells, insulin can hardly permeate the epithelial cell layer in the intestine. Meanwhile, the tight junctions (TJs) between epithelial cells prevent para-cellular transport of insulin.[7] To improve the oral bioavailability of insulin, these multiple absorption barriers have to be overcome simultaneously.

Previously, several strategies were used to improve oral insulin absorption.[8−13] Among these strategies, nanoparticles (NPs) may represent the most promising approach. Protein drugs encapsulated in nanoparticles are protected from enzymatic degradation in the GI tract. Moreover, the permeability of protein drugs through the mucus or epithelial cell barrier is enhanced due to the greater surface-area-to-volume ratio of

Received: April 24, 2015
Accepted: June 25, 2015
Published: June 25, 2015

DOI: 10.1021/acsami.5b03555
ACS Appl. Mater. Interfaces 2015, 7, 15430−15441

nanoparticles or the modification of nanoparticles' surface properties.[7,13,14]

Polylactide-*co*-glycoside (PLGA) is approved by the U.S. FDA and has been proven to be safe for clinical applications. PLGA nanoparticles (PLGA NPs) have gained numerous popularities in drug delivery.[15,16] Controlled release can be achieved by using PLGA NPs to protect effectively encapsulated protein drugs from enzymatic degradation in the GI tract.[17−22] However, the penetration of PLGA NPs through the mucus and epithelial barriers is poor because the negative surface charge of PLGA NPs limits the nanoparticles' interactions with the negatively charged mucus layer or cell membrane.[17−20] Coating by cationic polymers through electrostatic interactions could be an effective method for modifying the surface charge of PLGA NPs.

N-Trimethyl chitosan chloride (TMC) is a partially quaternized derivative of chitosan and can be prepared by reductive methylation.[23,24] The positive charge, good solubility and permeation-enhancing ability of TMC are maintained in neutral-pH environments, where chitosan is insoluble and ineffective as a permeation enhancer.[25,26] As previously reported, insulin loaded TMC nanoparticles (TMC NPs) were most commonly prepared by ionic cross-linking method.[27−30] In the process of preparation, the TMC NPs were formed by self-assembly of cationic TMC and oppositely charged insulin or by addition anionic low molecular cross-linker, such as tripolyphophate (TPP) to positively charged TMC. It was reported that the insulin loaded TMC NPs possess a positively charged surface and showed good mucoadhesive and intestinal epithelium-penetrating properties.[29] However, TMC NPs disintegrate easily because the electrostatic interaction between negatively charged insulin and positively charged TMC decreases in media with an ionic strength as high as that of intestinal fluid, resulting in the fast release of insulin. In fact, up to 50% of encapsulated insulin is released from TMC NPs in PBS in just 1 h.[30] With the presence of enzymes in the GI tract, this release could be even faster due to enzymatic degradation of the TMC NPs prepared by ionic cross-linking method. Although para-cellular transport of insulin is enhanced by the TJ-opening effect of TMC,[29] the limited area of TJs relative to the intestinal epithelia still makes it difficult for considerable amounts of insulin to be released to effectively permeate the epithelial cell barrier. As a result, the released insulin has poor absorption efficiency and undergoes enzymatic degradation in the intestinal lumen. It was indicated that although TMC NPs prepared by ionic cross-linking method is beneficial for overcoming the mucus and epithelial cell barriers to oral insulin absorption, the ability of the nanoparticles to overcome enzyme barrier need to be improved.

In our study, TMC coating of PLGA NPs was applied to combine the controlled-release property of PLGA NPs with the mucoadhesive and permeation-enhancing capacity of TMC. Insulin is encapsulated in the PLGA core. Meanwhile, TMC coating of the PLGA core is realized by electrostatic interactions between the negatively charged surface of PLGA core and cationic TMC. Protection of insulin in the GI tract is specifically achieved by the controlled release of insulin from our prepared TMC-coated PLGA nanoparticles (TMC-PLGA NPs) to overcome the enzyme barrier to oral insulin absorption. Moreover, it is hypothesized that the mucus barrier can be overcome by mucoadhesion of the TMC-PLGA NPs, followed by mucus penetration, and that the epithelial barrier can be overcome by improved cellular internalization of cationic TMC-PLGA NPs and enhanced para-cellular transport of insulin. By overcoming these multiple absorption barriers, oral administration of insulin-loaded TMC-PLGA NPs (Ins TMC-PLGA NPs) is expected to improve the bioavailability of insulin.

The effects of TMC-PLGA NPs on overcoming the multiple barriers to oral insulin absorption were evaluated both *in vitro* and *in vivo*. The protective ability of the nanoparticles was specifically evaluated based on the stability of the nanoparticles and the release of insulin in simulated gastrointestinal fluids. In addition, mucus-producing HT29-MTX cells were applied for *in vitro* evaluations of the mucus-penetrating capacity of the nanoparticles, and Caco-2 cell monolayers were used to investigate the epithelia-permeating ability of the nanoparticles. Furthermore, the mucoadhesive effect of the TMC-PLGA NPs was evaluated in mice. Finally, the hypoglycemic effect and relative pharmacological availability of the nanoparticles were tested in diabetic rats.

2. EXPERIMENTAL METHODS

2.1. Materials and Animals. Lakeshore poly(lactic-*co*-glycolic acid) (PLGA, lactic acid:glycolic acid = 50:50 and molecular weight of 20 000 Da) was kindly provided by Evonik, GmbH. (Evonik, Germany). Emprove exp poly(vinyl alcohol) (PVA) 4-88 was given as a present from Merck, GmbH. (Merck, Darmstadt, Germany). *N*-Trimethyl chitosan (TMC, viscosity 10−50 mPa·s, degree of deacetylation 85%, degree of trimethyl substitution 50%) was purchased from Xingzhongcheng Chemical Co., Ltd. (Hubei, China). Porcine insulin (27 IU/g) was obtained from Wanbang Biochemical Co., Ltd. (Jiangsu, China). ^{125}I or Rhodamine B labeled insulin was provided by Prof. Jianhua Zhu and Prof. Cong Li, respectively (School of Pharmacy, Fudan University). Fluorescent FPR648 labled PLGA (lactic acid:glycolic acid = 50:50 and molelular weight of 20 000 Da) was purchased from PolySciTech (West Lafayette, IN, USA). Corning Cellgro phosphate-buffered saline (PBS), Hank's balanced salt solution (HBSS), 0.25% (w/v) trypsin-EDTA and Dulbecco's modified essential medium (DMEM) were all purchased from Mediatech, Inc. (VA, USA). Cell culture plates were from Corning (Corning, NY, USA). *N*-Acetyl-L-cysteine (NAC) was obtained from Aladdin Chemistry Co., Ltd. (Shanghai, China). Gibco fetal bovine serum (FBS), Alexa Fluor 488 labeled wheat germ agglutinin (WGA) and Alexa Fluor 488 labeled donkey antigoat IgG were purchased from Life tech Inc. (Life technologies, Carlsbad, CA, USA). Occludin goat polyclonal IgG were obtained from Santa Cruz Biotechnology, Inc. (Dallas, Texas, USA). The pepsin, pancreatin and other chemicals were purchased from Sigma (St. Louis, MO, USA).

Caco-2 cells were obtained from American Type Culture Collection (Manassas, VA, USA). HT29-MTX cell line was a kind gift from Dr. Thecla Lesuffleur (INSERM, Paris, France).

Male Wistar rats weighing 200 ± 20 g and male Kunming mice weighing 20 ± 2 g were obtained from Sino-British SIPPR/BK Lab. Animal Co., Ltd. (Shanghai, China). All animal experiments were performed according to the Guiding Principles for the Care and Use of Experiment Animals in Fudan University (Shanghai, China). The protocols of the study were evaluated and approved by the ethical committee of Fudan University.

2.2. Preparation of NPs. Insulin loaded PLGA NPs (Ins PLGA NPs) were prepared using a double emulsion method, with slight modification from a method described previously.[31] Briefly, 0.2 mL of 20 mg·mL^{-1} insulin PBS solution was added to 1 mL of ethyl acetate containing 20 mg of PLGA. A W/O primary emulsion was formed after ultrasound sonication (200 W) for 30 s in ice bath. Then 2 mL of 2% (W/V) PBS solution of poly(vinyl alcohol) (PVA) was added and mixed by shaking out thoroughly followed by ultrasound sonication (200 W) for 30 s in ice bath to produce a W/O/W double emulsion. The double emulsion was added dropwise into 8 mL of 2% PBS solution of PVA, and the solution was mixed by magnetic stirring for 1 h at room temperature. The residual ethyl acetate was removed under vacuum rotary evaporation at 40 °C. Aliquots of the NPs suspension were washed twice with PBS by centrifugation (15000*g*, 4 °C, 30 min) and resuspension.

DOI: 10.1021/acsami.5b03555
ACS Appl. Mater. Interfaces 2015, 7, 15430−15441

Insulin loaded TMC-PLGA NPs (Ins TMC-PLGA NPs) were prepared by the same method as above except that cationic TMC (0.8 mg) was dissolved in 2 mL of a 2% (w/v) PBS solution of PVA as the outer water phase to form double emulsion (W/O/W).

2.3. Characterization of NPs. The size and ζ-potential of NPs were measured by Malvern Zetasizer Nano ZS (Malvern Instruments, Worcestershire, UK). The mean particle size, polydispersion index (PDI) of size and ζ-potential were recorded. All measurements were performed in triplicate. Morphological examination of PLGA NPs or TMC-PLGA NPs were performed using a transmission electron microscope (Tecnai G2 20, FEI, USA).

To determine the encapsulation efficiency (EE) and drug loading capacity (DLC), the insulin-loaded nanoparticles were separated from the aqueous suspension medium by ultracentrifugation at 15000*g* and 4 °C for 30 min. The amount of free insulin in the supernatant was determined using ultraperformance liquid chromatography (UPLC) (Waters Acquity UPLC H Class, Waters Corporation, USA). The UPLC system comprised a quaternary solvent manager, a TUV detector and a Acquity UPLC BEH C_{18} column (50 × 2.1 mm, 1.7 μm, 130 Å) to separate insulin. The mobile phase was a mixture of water, acetonitrile and trifluoroacetic acid with the ratio of 68.5:31.5:0.1. The flow rate was 0.3 mL/min and the detection wavelength was set at 214 nm. Aliquot 1 μL of the supernatant was injected into the UPLC system. The peak area of insulin was recorded and the concentration of free insulin in the supernatant was calculated from a standard curve. The EE and DLC were calculated using the following formula:

$$\text{encapsulation efficiency (EE) (\%)} = \frac{\text{total amount of insulin added} - \text{free insulin}}{\text{total amount insulin added}} \times 100\%$$

$$\text{drug loading capacity (DLC) (\%)} = \frac{\text{total amount of insulin added} - \text{free insulin}}{\text{weight of nanoparticles}} \times 100\%$$

2.4. Stability of NPs in Simulated Gastrointestinal Fluids. Simulated gastric fluid without pepsin (SGFsp), simulated intestinal fluid without pancreatin (SIFsp), pepsin-containing simulated gastric fluid (SGF) and pancreatin-containing simulated intestinal fluid (SIF) were prepared according to USP35. The SGF and SIF were 35 mM NaCl, 80 mM HCl, 0.3% (w/v) pepsin, pH 1.2 and 50 mM KH_2PO_4, 15 mM NaOH, 1.0% (w/v) pancreatin, pH 6.8, respectively. Aliquots of Ins PLGA NPs or Ins TMC-PLGA NPs were dispersed in SGFsp, SIFsp, SGF and SIF respectively at a concentration of 0.2 mg/mL. After incubation at 37 °C under agitation at 100 rpm on an orbital shaker for 2 h, nanoparticles were collected by ultracentrifugation and resuspended in water. The mean particle size and ζ-potential of each sample were measured as described above and were compared with the initial data before incubation.

2.5. *In Vitro* Drug Release From NPs. The method we used was slightly modified from a previous report.[20] The *in vitro* release profiles were studied with 0.2 mg/mL ^{125}I-labeled insulin (^{125}I-Ins) loaded NPs in SGFsp, SIFsp, SGF and SIF, respectively at 37 °C under agitation at 100 rpm. At predetermined times, samples were collected and centrifuged. The radioactivity of ^{125}I-Ins in the supernatant was counted (Wallac Wizard 1470 Gamma counter, PerkinElmer, Waltham, MA, USA). The release percent of ^{125}I-Ins from the NPs was then calculated by dividing the counts in the supernatant by the total counts of the nanoparticles added.

2.6. Cell Culture. The human colon adenocarcinoma cell lines, Caco-2 and HT29-MTX cells, were cultivated separately in 75 cm^2 culturing flasks containing 10 mL of Dulbecco's Modified Medium (DMEM, Corning Cellgro, Mediatech, USA) supplemented with 10% nonessential amino acid, 10% L-glutamine, 1% penicillin (100 IU/mL) and streptomycin (100 μg/mL) and 10% fetal bovine serum. Cells were maintained in an incubator at 37 °C, 95% relative humidity and 5% CO_2. The culture medium was replaced with fresh one every other day until the cells reached 60−80% confluence. Cells were then detached from the culturing flask by trypsin treatment and resuspended in fresh culture medium. For cellular uptake studies, cells were seeded onto 24-well plates (Corning, NY, USA) at a density of 5 × 10^4 cells/cm^2 and cultured for 14 days. For the permeation studies on cell monolayers, Caco-2 cells were seeded onto the Millicell hanging cell culture insert (PET membrane, pore size 0.4 μm) (Millipore Corporation, Billerica, MA, USA). The hanging cell culture inserts were placed into 24-well plates. The cells were allowed to grow and differentiate for 21 days before use. Caco-2 cells with passage numbers between 20 and 30 and HT29-MTX cells between 14 and 20 were used.

2.7. Study of Mucoadhesion and Mucus-Penetration Using HT29-MTXCells. HT29-MTX cells were seeded onto glass-bottomed cell culture dish for CLSM visualization (Nest Biotechnology Co., Ltd., Wuxi, China) at a density of 5 × 10^4 cells/cm^2 and were cultured for 14 days. Insulin was labeled with fluorescein Rhodamine B (RB-Ins) and fluorescein FPR648 labeled PLGA (FPR648-PLGA) were used in nanoparticles preparation for *in vitro* visualization. Cells were rinsed with HBSS, allowed to equilibrate at 37 °C for 20 min and then incubated with 500 μL of suspension of RB-Ins loaded FPR648-PLGA NPs or TMC-FPR648-PLGA NPs in HBSS (at a concentration of 500 μg/mL of RB-Ins) at 37 °C, 5% CO_2 for 2 h. Subsequently, the cells were washed with ice-cold PBS and counter-stained with Alexa Fluor 488 labeled wheat germ agglutinin (WGA) (5 μg/mL) for 15 min and bis-benzimide H33342 trihydrochloride (5 μg/mL) for 20 min. After that, samples were washed with PBS and examined under confocal laser scanning microscopy (CLSM, LSM710, Cal Zeiss, Jena, Germany). The images of nanoparticles or RB-Ins in the cell mucus layer or in the cell were captured.

To evaluate the influence of cell mucus layer on the absorption of nanoparticles, the mucus layer of HT29-MTX cells was removed prior to the experiment, with slight modification from a method described previously.[32] Briefly, HT29-MTX monolayers were washed with 10 mM *N*-acetyl cysteine (NAC) HBSS and incubated under agitation at 150 rpm for 1 h. Subsequently, the cells with mucus layer (without treatment of NAC, the control group) along with the cells without mucus layer (after treatment of NAC, the NAC group) were washed by HBSS for 3 times and treated with RB-Ins PLGA NP or TMC-PLGA NPs suspension (at a concentration of 500 μg/mL of RB-Ins) in HBSS at 37 °C, 5% CO_2 for 2 h. After that, the cells were washed to remove the unassociated nanoparticles. To measure the amount of drug that penetrated the cell mucus layer and entered the cells, the cells were treated with a 3% (v/v) formalin solution (the formalin group) to remove the mucus layer as previously reported.[33] The cell lysis was accomplished in cells of all groups by ultrasound sonication (200 W, 2 s each time at a 2 s interval, 40 times) in ice bath. The amount of RB-Ins was quantified by fluorescence analysis using a microplate reader (Infinite 200 PRO microplate reader, Tecan, Switzerland) with an excitation wavelength of 566 nm and an emission wavelength of 590 nm. The protein concentration of the cell lysis was determined using a bicinichoninci acid (BCA) assay kit (Beyotime Institute of Biotechnology, Jiangsu, China). The amount of cellular uptake of RB-Ins by HT29-MTX cells was expressed as the amount of RB-Ins associated with 1 mg of cellular protein.

2.8. Cellular Uptake Study Using Caco-2 Cells. Caco-2 cells were seeded onto glass-bottomed cell culture dish for CLSM visualization (Nest Biotechnology Co., Ltd., Wuxi, China) at a density of 5 × 10^4 cells/cm^2 and were cultured for 14 days. Cells were rinsed with HBSS, allowed to equilibrate at 37 °C for 20 min and then incubated with 500 μL of a 500 μg/mL RB-Ins loaded FPR648-PLGA NPs or TMC-FPR648-PLGA NPs suspension in HBSS (at a concentration of 500 μg/mL of RB-Ins) at 37 °C, 5% CO_2 for 2 h. In addition, RB-Ins solution at the same concentration was set as control. After that, the cells were washed 3 times with ice-cold PBS to remove the unassociated nanoparticles. Cells were counter-stained with DAPI (4′6-diamidino-2-phenylindole) (5 μg/mL) for 10 min under light exclusion. Samples were washed with PBS and examined under CLSM (LSM710, Cal Zeiss, Jena, Germany). The intracellular CLSM images were captured.

To evaluate quantitatively the cellular uptake of RB-Ins, Caco-2 cells were treated with RB-Ins PLGA NP or RB-Ins TMC-PLGA NPs suspension (at a concentration of 500 μg/mL of RB-Ins) in HBSS at 37 °C, 5% CO_2 for 2 h. In addition, RB-Ins solution at the same

DOI: 10.1021/acsami.5b03555
ACS Appl. Mater. Interfaces 2015, 7, 15430−15441

Table 1. Mean Size, Polydispersity Index (PDI), ζ-Potential, Encapsulation Efficiency (EE) and Drug-Loading Capacity (DLC) of Nanoparticles (n = 3)

nanoparticles	size (nm)	PDI	ζ-potential (mV)	EE (%)	DLC (%)
Ins PLGA NPs	132.4 ± 5.8	0.139 ± 0.046	−8.9 ± 3.4	48.0 ± 3.5	8.5 ± 0.6
Ins TMC-PLGA NPs	247.6 ± 7.2	0.242 ± 0.074	45.2 ± 4.6	47.0 ± 2.9	7.8 ± 0.5

concentration was set as control. Then cells were washed to remove the unassociated nanoparticles. The cell lysis was performed and the fluorescence intensity and protein concentration of the cell lysis were determined in the same way as described above. The amount of cellular uptake of RB-Ins by Caco-2 cells was expressed as the quantity of RB-Ins associated with 1 mg of cellular protein.

2.9. Mechanism of Cellular Uptake in Caco-2 Cells. To identify the possible cellular uptake mechanism of nanoparticles by Caco-2 cells, the cells were incubated in different conditions or treated with specific agents, with slight modification from a previously described method.[29,33] Briefly, 100 mM sodium azide, 10 μg/mL chlorpromazine, 5 μg/mL filipin III, 10 μg/mL cytochlalasin-D or 1 mM protamine sulfate was respectively dissolved in the suspension of nanoparticles and incubated with cells for 2 h at 37 °C. To test the effect of temperature on cellular uptake, cells were incubated with suspension of nanoparticles at 4 °C for 2 h. In addition, the control samples were conducted at 37 °C for 2 h without any treatment. The results of inhibition tests were presented as the percentage of cellular uptake amount of RB-Ins relative to the control group.

2.10. Transport through Caco-2 Cell Monolayers. The measurement of transepithelial electrical resistance (TEER) value and the transcelluar investigation of insulin through Caco-2 cell monolayers were carried out by a method slightly modified from a previous report.[34] Prior to the transport study, the medium in the apical and basolateral chambers were replaced with prewarmed fresh HBSS. The cells were rinsed with HBSS and allowed to equilibrate at 37 °C for 20 min. Then media in the apical chamber were replaced with 0.1 mL of suspension of RB-Ins PLGA NPs or RB-Ins TMC-PLGA NPs (RB-Ins at a concentration of 500 μg/mL). At predetermined time intervals, 0.2 mL of samples were collected from the basolateral chamber. The amount of RB-Ins transported was determined as described above and the percentage of RB-Ins transported through the cell monolayers was calculated.

The apparent permeability coefficients (P_{app}, cm/s) of RB-Ins were calculated according to the following equation:

$$P_{app} = \frac{Q}{A \times C \times t}$$

where Q is the total amount of insulin permeated (ng), A is the diffusion area of the cell monolayers (cm^2), c is the initial concentration of the insulin in the donor compartment (ng/cm^3) and t is the total time of the experiment (s).

At certain time intervals, the TEER values were measured by Millipore Millicell-Electrical Resistance System (Millipore Corporation, MA, USA). After incubation with nanoparticles for 2 h, the cell monolayers were washed by PBS to remove the nanoparticles and subsequently cultured in fresh cell culture media. The TEER values were measured at predetermined time intervals in the next 22 h. The percentage of TEER values relative to the initial level was calculated.

2.11. Immunofluorescence Imaging of Occludin Protein. Caco-2 cells were grown on Transwell permeable supports (polyester membrane, pore size of 0.4 μm, Corning, NY, USA) for 21 days to confluence and treated by FPR648-PLGA NPs or TMC-FPR648-PLGA NPs suspension. Occludin protein was stained using the immunofluorescence method as reported previously.[34] In brief, cells were fixed in 10% formalin, permeabilized in 1% BSA 0.4% Triton-X PBS and treated with 5% donkey serum PBS for 1 h to block nonspecific binding. The occludin goat polyclonal IgG at a concentration of 1:1000 was applied to the cells at 4 °C overnight. After the washing steps, cells were treated by Alexa Fluor 488 labeled donkey antigoat IgG (1:100 in PBS) for 1 h at room temperature. Subsequently, cells were viewed using CLSM for the tight junctions.

2.12. *In Vivo* Intestinal Mucoadhesion Study. Male Kunming mice weighing 20 ± 2 g were fasted overnight, but with free access to water before the experiment. ^{125}I-Ins PLGA NPs or ^{125}I-Ins TMC-PLGA NPs was administrated by intragastric gavage. After a predetermined time, the mice were sacrificed by cervical dislocation. An incision was made in the abdomen. The small intestine and colon were separated. In particular, the small intestine from the upper duodenum to the lower ileum was divided into four segments equal in length. All the intestinal segments were washed in normal saline. After that, the radioactive intensity was measured by γ-radioactive counter. The percentage of radioactive intensity of each intestinal segment to the total was calculated.

2.13. Pharmacodynamics Study in Diabetic Rats. The method we used is slightly modified from that of a previously reported method.[35] Male Wistar rats weighing 200 ± 20 g were fasted for 24 h, but with free access to water before intraperitoneal injection of streptozotocin (STZ) at a dose of 60 mg/kg to induce diabetes. Rats were regarded to be diabetic when their fasting blood-glucose level was higher than 15 mmol/L 1 week after the streptozotocin injection.

The diabetic rats were fasted overnight before administrated with the following formulations: oral administration of Ins PLGA NPs (at the insulin dose of 20 IU/kg), Ins TMC-PLGA NPs (at the insulin dose of 20 IU/kg), Ins solution (50 IU/kg) and PBS by intragastric gavage and subcutaneous injection of Ins solution (2 IU/kg). Before and at predetermined time intervals after dosing, one-drop-of-blood samples were collected from the caudal vein and the blood glucose concentration was measured as previously described.[35] The change in blood glucose concentration, represented by percentage to the initial value before the administration, was plotted against time. The biological activity of insulin or insulin loaded nanoparticles was calculated by dividing the blood glucose percentage by the corresponding blood glucose percentage in the control group (PBS ig. group). The area above the curve (AAC) was calculated using the trapezoidal method and was used to calculate the pharmacological availability (PA) according to the following equation:

$$PA = \frac{AAC \times dose_{sc.}}{AAC_{sc.} \times dose} \times 100\%$$

2.14. Statistical Analysis. Data were presented as the mean ± standard deviation. t test and one-way analysis of variance (ANOVA) were used to determine significance between two groups and among more than two groups, respectively. A value of $P < 0.05$ was considered to be significant.

3. RESULTS

3.1. Characterization of NPs. The mean particle size of the Ins TMC-PLGA NPs tested by dynamic light scattering was about 100 nm greater than that of Ins PLGA NPs (Table 1). Similar results in particle size was shown in the TEM images of PLGA NPs and TMC-PLGA NPs (Figure 1). Whereas Ins PLGA NPs had a negative ζ-potential, the surface of Ins TMC-PLGA NPs was positively charged. It was indicated that the PLGA NPs were successfully coated with cationic TMC. The encapsulation efficiency (EE) and drug-loading capacity (DLC) of the TMC-PLGA NPs showed no significant differences from those of the PLGA NPs ($P > 0.05$).

3.2. Stability of NPs in Simulated Gastrointestinal Fluids. To evaluate the stability of the nanoparticles in the GI tract, changes in the mean particle size and ζ-potential of the nanoparticles after incubation in simulated gastrointestinal fluids

DOI: 10.1021/acsami.5b03555
ACS Appl. Mater. Interfaces 2015, 7, 15430−15441

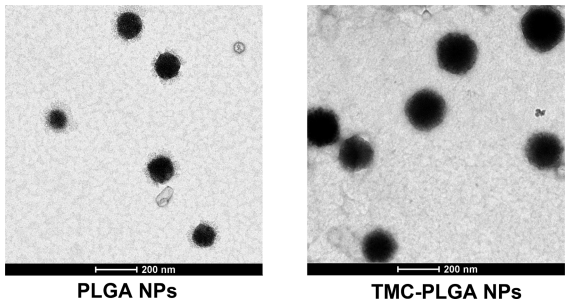

Figure 1. TEM images of PLGA NPs and TMC-PLGA NPs.

were measured. No significant changes in the mean particle size or ζ-potential of the nanoparticles were found after incubation in the enzyme-free SGFsp or SIFsp for 2 h, suggesting that most of the nanoparticles remained intact (Figure 2A). In contrast, the

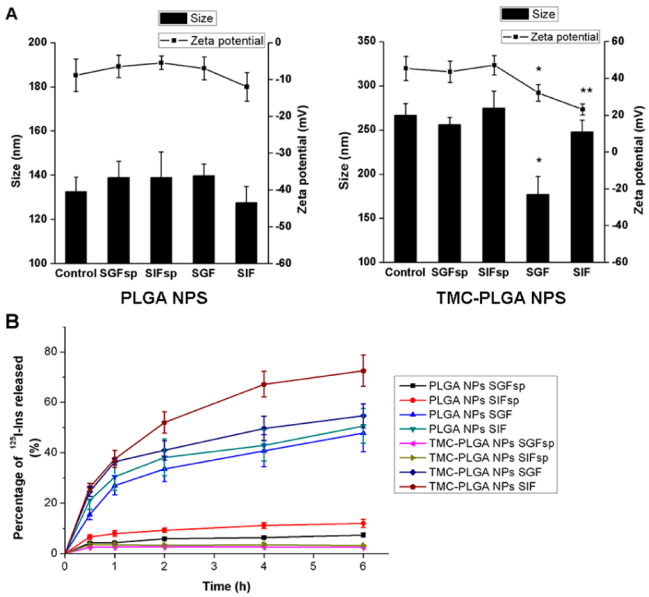

Figure 2. (A) Size and ζ-potential of PLGA NPs and TMC-PLGA NPs after 2 h of incubation in SGF without pepsin (SGFsp), in SIF without pancreatin (SIFsp), in SGF with pepsin (SGF) or in SIF with pancreatin (SIF) (n = 3). The size and ζ-potential of the nanoparticles before incubation served as the control. Significant differences are denoted as follows: *, $P < 0.05$, compared with the control group; **, $P < 0.01$, compared with the control group. (B) Profiles of *in vitro* ^{125}I-Ins release from PLGA NPs and TMC-PLGA NPs in SGFsp, in SIFsp, in SGF or in SIF (n = 3). Insulin labeled with the radioactive isotope ^{125}I was encapsulated in the nanoparticles used in the *in vitro* release study.

stability of the TMC-PLGA NPs was impaired after contact with enzymes, as indicated by a significant decrease in the ζ-potential in enzyme containing SGF and SIF and a significant decrease in the mean particle size in SGF.

3.3. *In Vitro* Drug Release From NPs. Because insulin is vulnerable to pepsin or pancreatin in gastrointestinal fluid, the ability of nanoparticles to protect insulin from degradation could be evaluated *in vitro* by determining the profile of insulin release from NPs in SGF or SIF. ^{125}I-labeled insulin was used in the *in vitro* release tests because the radioactive isotope ^{125}I is not affected by the proteases in the release medium. Thus, the amount of insulin released into the enzyme-containing release medium was determined from the radioactive intensity of ^{125}I. Less than 10% of the ^{125}I-Ins encapsulated in the nanoparticles was released after incubation in enzyme-free SGFsp or SIFsp for 6 h (Figure 2B). In particular, the release of ^{125}I-Ins from TMC-PLGA NPs was significantly slower than those from PLGA NPs. The release was much faster when enzymes were present in the release medium. In particular, the release profiles were biphasic, with a burst release of less than 10% of the drug in enzyme-free SGFsp or SIFsp and approximately 30% of the drug from enzyme-containing SGF or SIF during the first 1 h, followed by more sustained release over the next 5 h. Although no significant differences were observed between the cumulative release of insulin from TMC-PLGA NPs in SGF (36.5 ± 1.3%) and in SIF (37.5 ± 3.4%) in the burst-release phase, after 6 h, the release of insulin in SIF (72.5 ± 6.2%) was significantly higher than that in SGF (54.6 ± 4.7%). As illustrated, approximately 30−50% of the drug remained in the nanoparticles after the release profile reached a plateau, with the nanoparticles protecting the insulin from enzymatic degradation.

3.4. Study of Mucoadhesion and Mucus Penetration Using HT29-MTX Cells. The mucoadhesive and mucus-penetrating properties of the nanoparticles were evaluated using the mucus-secreting HT29-MTX cell model. Specifically, the mucus layer covering the cells was characterized by staining with fluorescence-labeled wheat germ agglutinin (WGA) (green signal in Figure 3A). The distribution of insulin and nanoparticles in the mucus layer and inside the HT29-MTX cells after incubation with Rhodamine B (RB)-Ins TMC-FPR648-PLGA NPs or FPR648-PLGA NPs is shown in Figure 3A. When the same initial amount was used, more TMC-FPR648-PLGA NPs (yellow signal) than FPR648-PLGA NPs were attached to the mucus layer (green signal), suggesting that the mucoadhesive effect was enhanced after TMC coating. It is demonstrated that more TMC-FPR648-PLGA NPs (yellow signal) penetrated the mucus layer and entered the cells, illustrating the stronger mucus-penetrating capacity of the TMC-coated nanoparticles. Moreover, the red signal of the drug highly overlapped with the yellow signal of PLGA in the mucus layer or in the cells, indicating that the accumulation of insulin in the mucus layer was attributable to the bioadhesive ability of the nanoparticles.

The distribution of drug in the mucus layer and cell monolayers was measured quantitatively, and the results are shown in Figure 3B. To characterize the mucoadhesive property of the nanoparticles, the amounts of cellular uptake of insulin in the control group and the *N*-acetylcysteine (NAC) group were compared. However, no significant difference was found between the amounts of cellular uptake of RB-Ins in the control group and the NAC group for the PLGA NPs, indicating that the PLGA NPs were not mucoadhesive. Moreover, the amount of RB-Ins that penetrated the mucus layer and entered the cells (the amount of cellular uptake in the formalin group) was relatively low for the PLGA NPs, which was confirmed by the weak intensity of the RB-Ins signal in the cells observed by CLSM (Figure 3A). This poor mucus penetration of the PLGA NPs may have resulted from their poor mucoadhesion.

After treatment with TMC-PLGA NPs, the uptake of RB-Ins by HT29-MTX cells in the control group was 28% higher than that in the NAC group, indicating better association of the TMC-PLGA NPs with the mucus layer than with the cell membrane. Moreover, the cellular uptake of RB-Ins in the control group was dramatically higher for TMC-PLGA NPs than for unmodified PLGA NPs, indicating great improvement in the association of the nanoparticles with the mucus after TMC coating. Furthermore, the fraction of insulin that penetrated the cell mucus layer and entered the cells (the amount of cellular uptake

DOI: 10.1021/acsami.5b03555
ACS Appl. Mater. Interfaces 2015, 7, 15430−15441

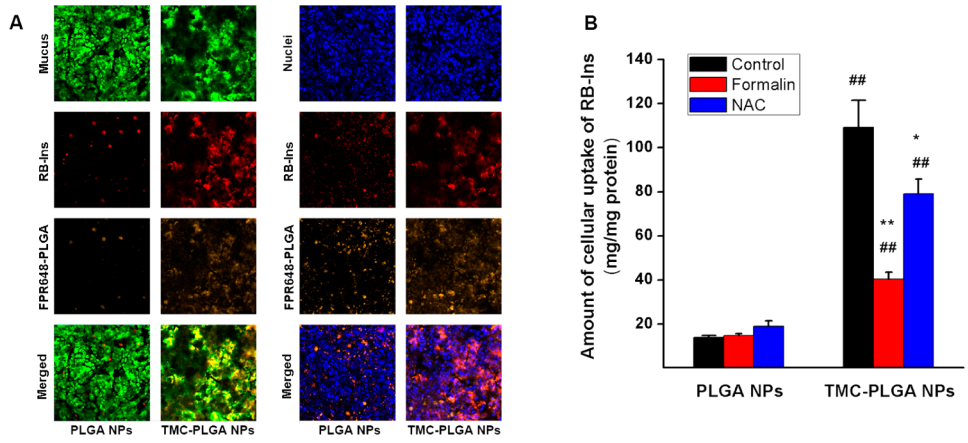

Figure 3. (A) CLSM images of mucus layers and cell layers of HT29-MTX cells treated with RB-Ins TMC-FPR648-PLGA NPs or RB-Ins FPR648-PLGA NPs for 2 h. The green signal in the first row represents the mucus stained with Alexa 488-WGA, the blue signal in the first row represents the nuclei stained with H33342, the red signal in the second row represents RB-Ins, the yellow signal in the third row represents FPR648-PLGA and the merged signals are in the fourth row. (B) Cellular uptake of RB-Ins by mucus-secreting HT29-MTX cells after treatment with RB-Ins TMC-PLGA NPs or PLGA NPs (n = 4−6). The amount of cellular uptake in the control group represented the amount of RB-Ins that was associated with the cell mucus layer or that entered the cells. The amount of cellular uptake in the NAC group represented the amount of association of RB-Ins with the HT29-MTX cells without a mucus layer. The amount of cellular uptake in the formalin group indicated the amount of RB-Ins that penetrated the cell mucus layer and entered the cells. Significant differences are denoted as follows: *, $P < 0.05$, compared with the control group; **, $P < 0.01$, compared with the control group; and ##, $P < 0.01$, compared with the Ins PLGA NP group.

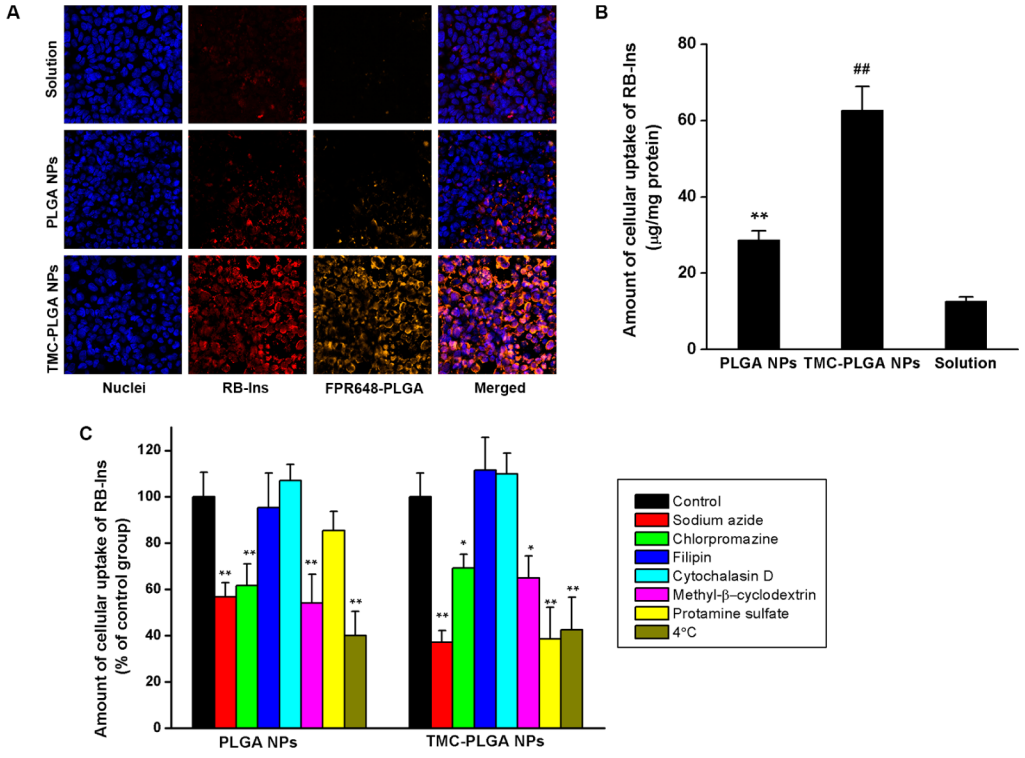

Figure 4. (A) CLSM images of Caco-2 cells treated with RB-Ins solution, RB-Ins FPR648-PLGA NPs, or RB-Ins TMC-FPR648-PLGA NPs. The blue signal represents nuclei stained with DAPI, the red signal represents RB-Ins and the yellow signal represents FPR648-PLGA. (B) Cellular uptake of RB-Ins PLGA NPs, TMC-PLGA NPs and RB-Ins solution by Caco-2 cells (n = 4−6). The amount of cellular uptake is expressed as the amount of RB-Ins internalized per cellular protein. Significant differences are denoted as follows: **, $P < 0.01$, compared with RB-Ins solution; ##, $P < 0.01$, compared with RB-Ins PLGA NPs. (C) Cellular uptake of RB-Ins by Caco-2 cells after incubation with RB-Ins PLGA NPs or TMC-PLGA NPs under different conditions (n = 4−6). Significant differences are denoted as follows: *, $P < 0.05$, compared with the control; **, $P < 0.01$, compared with the control.

in the formalin group) was 2-fold greater for TMC-PLGA NPs than for PLGA NPs, suggesting that the mucus penetration of insulin was significantly improved by TMC coating of nanoparticles.

3.5. Cellular Uptake Study Using Caco-2 Cells. An intestinal epithelium-like Caco-2 cell monolayer was established for the cellular uptake experiment. The CLSM images of the nanoparticles and drug internalized by Caco-2 cells are shown in Figure 4A. Meanwhile, the cellular uptake of RB-Ins was

DOI: 10.1021/acsami.5b03555
ACS Appl. Mater. Interfaces 2015, 7, 15430−15441

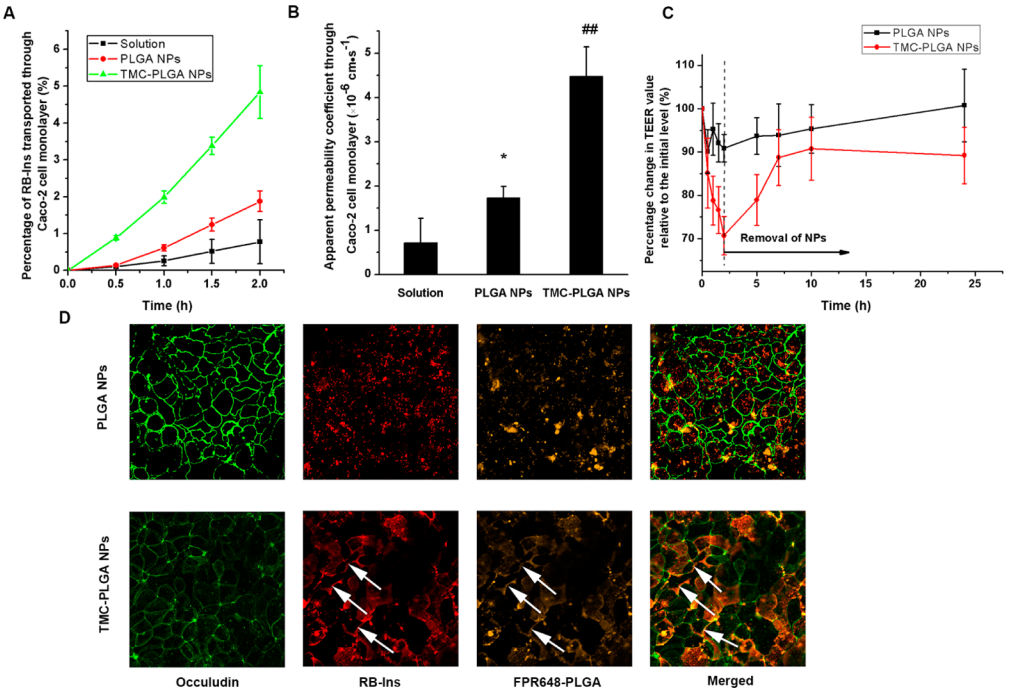

Figure 5. (A) Efficiency of RB-Ins transport through Caco-2 cell monolayers after treatment with RB-Ins PLGA NPs, RB-Ins TMC-PLGA NPs or RB-Ins solution ($n = 4–6$). (B) Apparent permeability coefficients of RB-Ins transport through Caco-2 cell monolayers ($n = 4–6$). Significant differences are denoted as follows: *, $P < 0.05$, compared with RB-Ins solution; ##, $P < 0.01$, compared with Ins PLGA NPs. (C) Percentage change in the TEER value relative to the initial level for Caco-2 cell monolayers. The nanoparticles were removed after 2 h of incubation and the cell monolayers were subsequently incubated in culture medium for 22 h ($n = 6$). (D) CLSM images of Caco-2 cells after incubation with RB-Ins FPR648-PLGA NPs or RB-Ins TMC-FPR648-PLGA NPs. The occludin protein in the TJs was stained with Alexa Fluor 488 (green). The red and yellow signals indicate RB-Ins and FPR648-PLGA, respectively. The areas marked by white arrows indicate the opened TJs, through which RB-Ins and FPR648-PLGA molecules were transported.

measured quantitatively and is shown in Figure 4B. Negligible RB-Ins signals were observed in the cells treated with RB-Ins solution, which confirmed that RB-Ins given in the form of a solution hardly entered the cells. The stronger signal of RB-Ins in the cells after incubation with RB-Ins PLGA NPs and the overlap of the PLGA and RB-Ins signals observed by CLSM indicated that the cellular internalization of RB-Ins was enhanced by encapsulation in the NPs. Consistent with this finding, the amount of cellular uptake of RB-Ins was significantly improved for the RB-Ins PLGA NPs compared with the RB-Ins solution.

Compared with the cells treated with PLGA NPs, in the cells treated with TMC-PLGA NPs, even stronger fluorescent intensity was observed, and a significantly higher amount of RB-Ins was taken up by the cells. These results suggested that the cellular uptake of nanoparticles is greatly enhanced by TMC coating.

The mechanism of uptake by Caco-2 cells was investigated under different conditions. As shown in Figure 4C, the amount of uptake of RB-Ins by the Caco-2 cells was significantly reduced at 4 °C and with the addition of sodium azide for both PLGA NPs ($P < 0.01$) and TMC-PLGA NPs ($P < 0.01$), as both of these conditions can block active transport processes. Methyl-β-cyclodextrin, an inhibitor of both clathrin-dependent and clathrin-independent cellular uptake, also significantly decreased the cellular uptake of PLGA NPs and TMC-PLGA NPs (approximately 45.9% reduction, $P < 0.01$; 35.1% reduction, $P < 0.05$, respectively). To determine further the relative involvement of clathrin-dependent endocytosis, chlorpromazine treatment was used to inhibit clathrin-dependent endocytosis. Overall, chlorpromazine inhibited the uptake of PLGA NPs and TMC-PLGA NPs to 61.7 ± 9.4% ($P < 0.01$) and 69.2 ± 5.8% ($P < 0.05$), respectively, in Caco-2 cells. Moreover, the caveolin-mediated endocytosis inhibitor filipin III and the pinocytosis inhibitor cytochalasin D, had no effect on the uptake of PLGA NPs and TMC-PLGA NPs by cells. Hence, these results demonstrated that clathrin-dependent endocytosis was involved in the cellular uptake of PLGA NPs and TMC-PLGA NPs and that there were no apparent direct roles for caveolae-dependent mechanisms or pinocytosis-dependent mechanisms.

Moreover, as an adsorption-mediated endocytosis inhibitor, protamine induced a strong decrease in cellular internalization, to 38.5 ± 13.6%, for TMC-PLGA NPs ($P < 0.01$). In contrast, the cellular uptake of PLGA NPs was not affected by protamine. These results implied that adsorptive endocytosis might play an important role in the uptake of TMC-PLGA NPs and probably accounts for these NPs' increased internalization compared with PLGA NP internalization.

3.6. Transport through Caco-2 Cell Monolayers. Figure 5A shows the cumulative amount of RB-Ins transported through Caco-2 cell monolayers incubated with RB-Ins solution, RB-Ins PLGA NPs or TMC-PLGA NPs as a function of time. The apparent permeability coefficient (P_{app}) of RB-Ins was calculated (Figure 5B). As shown, the cumulative amount of RB-Ins transported through the Caco-2 cell monolayers in the control group (RB-Ins solution) was negligible. The P_{app} value for RB-Ins from the TMC-PLGA NPs (4.48 ± 0.66 × 10^{-6} cm/s) was significantly greater than that for the PLGA NPs (1.74 ± 0.26 × 10^{-6} cm/s). These results indicated that TMC coating of PLGA NPs significantly enhanced insulin transport through Caco-2 cell monolayers.

As shown in Figure 5C, compared with PLGA NPs, incubation of TMC-PLGA NPs on the apical side of the Caco-2 cell

DOI: 10.1021/acsami.5b03555
ACS Appl. Mater. Interfaces 2015, 7, 15430–15441

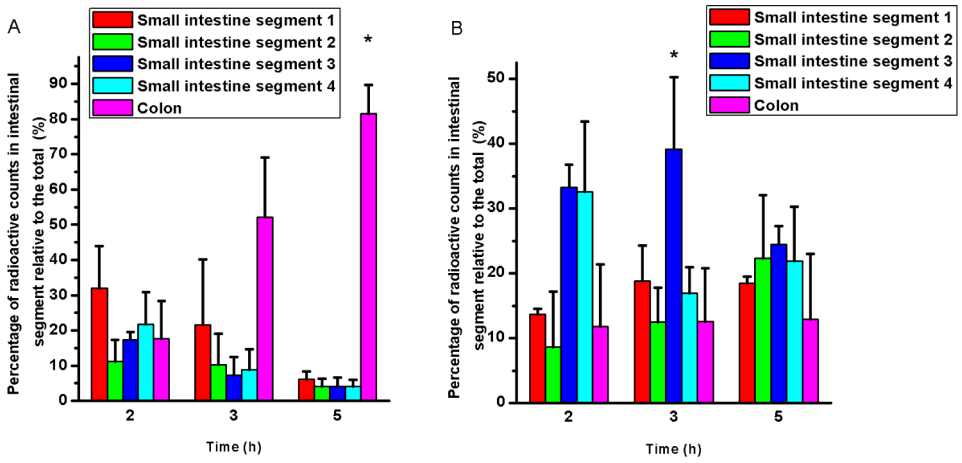

Figure 6. Distribution of radioactive counts in murine intestinal segments over time after oral administration of ^{125}I-Ins PLGA NPs (A) or ^{125}I-Ins TMC-PLGA NPs (B) (n = 6). Significant differences are denoted as follows: *, $P < 0.05$, compared with the radioactive counts in all of the other intestinal segments at the same time.

monolayers led to an immediate reduction in the trans-epithelial electrical resistance (TEER) value. After removal of the incubated TMC-PLGA NPs, a gradual increase in the TEER value was observed. These observations indicate that TMC-PLGA NPs might reversibly open the TJs between Caco-2 cells.

After incubation with RB-Ins FPR648-PLGA NPs or TMC-FPR648-PLGA NPs, the Caco-2 monolayers were immunofluorescently stained for occludin protein (Figure 5D). As shown by the weaker fluorescent signal of occludin protein, the expression of occludin protein was down-regulated after incubation with TMC-PLGA NPs compared with PLGA NPs. It was implied by the decrease in the TEER value and the down-regulation of occludin expression that the TJs were opened by the TMC-PLGA NPs. As illustrated in Figure 5D, the signals of insulin and PLGA were highly dispersed in the cells that were treated with PLGA NPs. In contrast, after TMC-PLGA NP treatment, the signals of insulin and PLGA tended to colocalize with occludin protein. It was indicated that with the TJs opened by the TMC-PLGA NPs, the insulin released from the TMC-PLGA NPs could be transported through a para-cellular pathway.

3.7. *In Vivo* Intestinal Mucoadhesion Study. To evaluate the mucoadhesive effects of nanoparticles, the distribution of nanoparticles labeled with the radioactive isotope ^{125}I in murine intestinal segments was investigated after oral administration. As shown in Figure 6, whereas most of the PLGA NPs administered moved to the colon 3 h after administration, approximately 40% of the TMC-PLGA NPs remained in the lower part of the small intestine. When coated with TMC, the movement of NPs along the intestine was much slower, implying that the TMC-coated nanoparticles had mucoadhesive properties.

3.8. Pharmacodynamics Study in Diabetic Rats. The effects of hypoglycemia were evaluated after oral administration of insulin-loaded nanoparticles to streptozotocin (STZ)-induced diabetic rats. As illustrated in Figure 7, no hypoglycemic effect was observed following oral administration of PBS solution, which was used as a negative control. The hypoglycemic effect following subcutaneous injection of 2 IU/kg insulin was used as a positive control to calculate the relative pharmacological availability (PA) of orally delivered insulin solution or nanoparticles. The blood glucose level (BGL) decreased significantly soon after subcutaneous injection of 2 IU/kg insulin.

After oral administration of 50 IU/kg insulin, no statistically significant decrease in the BGL was observed compared with the

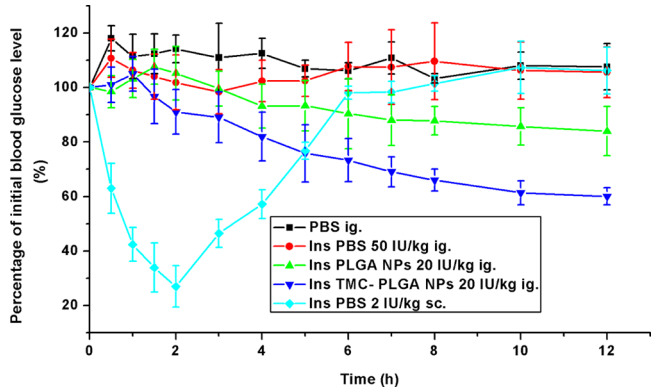

Figure 7. BGLs in diabetic rats following oral administration of Ins PLGA NPs or TMC-PLGA NPs at an insulin dose of 20 IU/kg or insulin solution at a dose of 50 IU/kg (n = 6). Oral administration of PBS served as a blank control and subcutaneous injection of insulin solution at a dose of 2 IU/kg was used as a positive control (n = 6).

negative control, suggesting that oral delivery of insulin solution was completely ineffective. However, oral administration of 20 IU/kg Ins PLGA NPs yielded a glucose-lowering effect, and the BGL gradually decreased to 85.7% of the initial level after 10 h, which was significantly lower than that in the negative-control group. Table 2 also shows that the PA of the orally administered Ins PLGA NPs relative to the subcutaneous injected insulin solution (5.93%) was significantly improved compared with that of orally delivered insulin solution (0.51%). These results demonstrated that encapsulation in nanoparticles could enhance the absorption of insulin.

The BGL decreased rapidly after oral administration of 20 IU/kg Ins TMC-PLGA NPs and reached 70% of the initial level after 7 h, which was significantly lower than in any of the previous groups. More importantly, the BGL continued to decrease over an extended period of 12 h, indicating a long-lasting hypoglycemic effect. In fact, if the experiments had not been terminated because the rats could not be fasted any longer, the hypoglycemic effect could have lasted longer than 12 h. Furthermore, the PA (11.82%) of the orally administered Ins TMC-PLGA NPs was substantially higher than that of the Ins PLGA NPs, indicating improved insulin absorption after TMC coating of the nanoparticles.

DOI: 10.1021/acsami.5b03555
ACS Appl. Mater. Interfaces 2015, 7, 15430−15441

Table 2. Calculated Pharmacodynamics Parameters of Diabetic Rats in Different Groups ($n = 6$)

parameter	Ins ig.	Ins PLGA NPs ig.	Ins TMC-PLGA NPs ig.	Ins sc.
dose (IU/kg)	50	20	20	2
$AAC_{0\rightarrow 12h}$(%h)	39.20 ± 85.58	181.35 ± 69.97	361.61 ± 57.98	306.01 ± 51.91
$PA_{0\rightarrow 12h}$(%)	0.51 ± 1.21	5.93 ± 3.29[a]	11.82 ± 3.90[b]	100.00 ± 33.93

[a]$P < 0.05$, compared with Ins ig. [b]$P < 0.05$, compared with Ins PLGA NPs ig.

4. DISCUSSION

We developed insulin-loaded TMC-coated PLGA nanoparticles to simultaneously overcome the multiple barriers to insulin absorption. The surface of PLGA NPs is negatively charged in neutral pH environment, as indicated by the negative ζ-potential (Table 1), whereas positive charges are displayed by the N-quaternized [$^{+}N(CH_3)_3$] groups of TMC.[25,26] TMC coating of PLGA NPs could be realized by electrostatic interactions between the negative charged surface of PLGA NPs and the cationic TMC. TMC has been successful coated on the surface of PLGA NPs, indicated by the significantly increased size and ζ-potential of TMC-PLGA NPs (Table 1).

Although nanoparticles shelter encapsulated insulin from proteases in the GI tract, the release of insulin from the nanoparticles leads to a loss of protection. Disintegration or degradation of nanoparticles in the gastrointestinal fluid may be one reason for this insulin release. Thus, in the current study, the *in vitro* release of insulin and the stability of the nanoparticles were investigated to evaluate the protective effect of the NPs.

Our results showed that both Ins PLGA NPs and TMC-PLGA NPs remained stable in enzyme-free SGFsp and SIFsp (Figure 2A). Because TMC remains cationic in the acid and neutral-pH environments,[25,26] the positive surface charge of our prepared TMC-PLGA NPs was maintained in SGFsp and SIFsp (Figure 2A), and no aggregations were observed. Meanwhile, the release of ^{125}I-Ins from both ^{125}I-Ins PLGA NPs and TMC-PLGA NPs in SGFsp and SIFsp was negligible (Figure 2B). In contrast, it was reported that over 30% of insulin was released from the TMC NPs prepared using the ionic cross-linking method after 1 h in similar enzyme-free medium.[30] Thus, better insulin protection could be realized by PLGA NPs or TMC-PLGA NPs in gastrointestinal fluids with high ionic strengths due to the better controlled release property. Moreover, the release of ^{125}I-Ins from TMC-PLGA NPs was significantly slower than that from PLGA NPs, indicating the effect of TMC coating of NPs on release control.

The *in vitro* release in enzyme-containing gastrointestinal fluids is regarded to correlate better with the real profiles of insulin release from nanoparticles in the GI tract. In our study, the release of ^{125}I-Ins from PLGA NPs and TMC-PLGA NPs was much faster in enzyme-containing SGF an SIF compared with enzyme-free SGFsp and SIFsp (Figure 2B). In addition, the stability of the nanoparticles was impaired in SGF and SIF, as reflected by the significantly decreased mean particle size or ζ-potential (Figure 2A). The reduction in size of the nanoparticles and the fast release of ^{125}I-Ins were probably caused by the acceleration of PLGA hydrolysis in the presence of the enzymes.[36,37] It was found by us that after incubation with 5% bovine serum albumin (BSA) solution, the mean particle size of both Ins PLGA NPs and Ins TMC-PLGA NPs were significantly increased while the ζ-potential decreased, probably due to protein adsorption on the surface of nanoparticles. It is likely that enzymes in SIF or SGF were adhered on the surface of nanoparticles, inducing an increase in mean particle size and a decreased in ζ-potential of the nanoparticles. Therefore, the changes of size and ζ-potential of PLGA NPs or TMC-PLGA NPs resulted from the overall effects of nanoparticle degradation and enzyme adsorption.

A biphasic release profile is shown in our study and has been shown by other researchers.[20,38,39] In the burst-release phase, the insulin attached to the nanoparticle surface was first released by PLGA degradation. The insulin then diffused slowly from the inner part of the nanoparticles during the second, slow-release phase, passing through the pores that were formed by PLGA degradation. In particular, significantly larger amount of ^{125}I-Ins was release from both TMC-PLGA NPs and PLGA NPs in the burst release stage in enzyme-containing SGF or SIF than that in SGFsp or SIGsp. It was speculated that the insulin adsorbed on the surface of nanoparticles might not be thoroughly released in the burst release stage in enzyme-free medium. However, faster and more thorough bust release of adsorbed ^{125}I-Ins was induced by the digestion of insulin and the surface area of nanoparticles in SGF or SIF.

Interestingly, the TMC-PLGA NPs showed pH-responsive release in enzyme-containing medium. More insulin was released from the TMC-PLGA NPs in SIF compared with SGF, particularly during the second release phase (Figure 2B). There are probably more enzymes adsorbed on the surface of TMC-PLGA NPs in SIF compared with SGF, as reflected by the significantly lower ζ-potential and unchanged mean particle size in SIF (Figure 2A). The accelerated release of insulin from the TMC-PLGA NPs in SIF compared with SGF was probably due to faster degradation of PLGA induced by more enzyme adsorption.

After the Ins PLGA NPs or TMC-PLGA NPs was incubated in SGF or SIF for 6 h, approximately 30−50% of the insulin remained in the nanoparticles, protected from enzymatic degradation (Figure 2B). Encapsulation in PLGA NPs or TMC-PLGA NPs could thus slightly overcome the enzymatic barrier to oral insulin absorption. However, with numerous enzymes in the intestinal lumen, the protective effects of nanoparticles remain limited and are not long lasting. Therefore, nanoparticles must penetrate the mucus layer and enter the epithelial cells before most of the insulin is released in the GI tract.

Both size and surface charge are important properties of nanoparticles that can affect the mucus-penetrating ability and cellular uptake of the nanoparticles. In the present study, after coating with TMC, the size of the nanoparticles increased to approximately 100 nm (Table 1), which could make mucus penetration and cellular internalization more difficult.[40] Meanwhile, the positive surface charge obtained after TMC coating (Table 1) could enhance the mucus penetration and cellular uptake of nanoparticles.[41,42] The overall effects of TMC coating on the mucus-penetrating ability, cellular uptake and transport of nanoparticles were specifically evaluated *in vitro* with various cell models, and we found that the mucus penetration of the NPs and the transport of insulin through the intestinal epithelium were improved by TMC coating of the NPs.

DOI: 10.1021/acsami.5b03555
ACS Appl. Mater. Interfaces 2015, 7, 15430−15441

The mucus association and penetration ability of the nanoparticles were evaluated using mucus-secreting HT29-MTX cells, which are derived from colorectal carcinoma.[33] This HT29-MTX cell model has been intensively used to evaluate the bioadhesion and mucus penetration properties of nanoparticles.[27,33] In the present study, the mucus layer of the HT29-MTX cells was characterized using fluorescence-labeled WGA staining. Only negligible amounts of PLGA NPs were entrapped in the cell mucus layer (Figure 3A). The relatively fast diffusion of the PLGA NPs through the cell mucus layer was probably due to the nearly neutrally charged surface. As reported by other researchers, nanoparticles with neutral surface charges move fast through mucus.[43] However, the amount of RB-Ins that penetrated the mucus layer and was internalized by the cells remained very low after PLGA NPs treatment. Therefore, although mucus layer penetration was not a rate-limiting step for absorption of the PLGA NPs, the poor association of the PLGA NPs with the mucus layer resulted in poor absorption.

It was reported that nanoparticles composed of mucoadhesive polymers, such as chitosan derivatives, can associate with the mucus layer through the formation of hydrogen bonds, van der Waals' forces, hydrophobic forces and electrostatic interactions.[5] The mucoadhesive property of the TMC-PLGA NPs was confirmed by the obviously more nanoparticles and larger amount of RB-Ins adhered with the mucus layer for TMC-PLGA NPs than for PLGA NPs (Figure 3A,B). Whereas relatively more TMC-PLGA NPs than PLGA NPs were entrapped in the mucus layer, significantly more RB-Ins from the TMC-PLGA NPs compared with the PLGA NPs could penetrate the mucus layer and enter the cells (Figure 3B). This result was attributed to the bioadhesive property of the TMC coating, which dramatically improved the association of the nanoparticles with the mucus layer, providing greater opportunity for mucus penetration. The mucus penetration enhancement by mucoadhesive properties of nanoparticles has also been reported by other researchers.[33]

The epithelial cell layer in the GI tract is another barrier to nanoparticle absorption. In our study, cellular uptake and transport of insulin across the mucosal barrier was examined using Caco-2 cell model, which have been widely applied as a reliable and high-throughput *in vitro* system for evaluating the intestinal absorption potential of drug candidates.[44] In the present study, cellular internalization of insulin was facilitated by endocytosis of the nanoparticles, as indicated by the stronger signal of RB-Ins inside the Caco-2 cells detected by CLSM (Figure 4A) and the larger amount of RB-Ins internalized by the cells for PLGA NPs or TMC-PLGA NPs than that for RB-Ins solution (Figure 4B). Compared with PLGA NPs, the cellular uptake of RB-Ins and nanoparticles after treatment with TMC-PLGA NPs notably increased, apparently due to the enhancement of nanoparticle endocytosis by the TMC coating. Adsorption-mediated endocytosis, a common route for the internalization of positively charged nanoparticles,[27] was specifically involved in the cellular uptake of TMC-PLGA NPs and was probably attributable to the increased internalization of TMC-PLGA NPs compared with PLGA NPs.

Transport of insulin through Caco-2 cell monolayers was further investigated to evaluate the ability of nanoparticles to penetrate the epithelial cell layer. Compared with Ins PLGA NPs, the apical to basolateral flux of RB-Ins through Caco-2 cell monolayers significantly increased after incubation with Ins TMC-PLGA NPs (Figure 5A). In agreement with these findings, the permeability coefficient of RB-Ins crossing Caco-2 cell monolayers was estimated to be 3- to 4-fold higher for RB-Ins TMC-PLGA NPs than for RB-Ins PLGA NPs (Figure 5B).

Reversible opening of TJs among Caco-2 cells after incubation with TMC-PLGA NPs was indicated by a reversible decrease in the TEER value (Figure 5C) and the down-regulation of occludin protein expression (Figure 5D). It has been reported that chitosan can reversibly open TJs among epithelial cells in acidic environments[45] and that TMC has an even stronger ability to open TJs.[26] Moreover, chitosan and its derivatives do not increase the absorption of endotoxin, so their effect on TJs is regarded as safe,[46] It was confirmed by the cytotoxicity results of our prepared TMC-PLGA NPs (Supporting Information Figure S1). Generally, the gap between intestinal epithelial cells is approximately 0.3−1 nm wide, and the width should increase to 20 nm even when the TJs are thoroughly opened. In principle, though, it is still difficult for intact nanoparticles to pass through via the para-cellular route.[23] Therefore, in Caco-2 cells treated with TMC-PLGA NPs, the fluorescent signal of PLGA, which overlapped with the TJ signal observed by CLSM, might not be regarded as a nanoparticle signal, but rather as a PLGA polymer signal (Figure 5D). The disintegration of TMC-PLGA NPs and the release of RB-Ins presumably occurred during incubation with Caco-2 cells, due to the digestion of nanoparticles by brush border enzymes expressed on the surface of the Caco-2 cells.[47] The colocalization of insulin with the TJs of the Caco-2 cells, as observed by CLSM, suggested that insulin released from the TMC-PLGA NPs could be transported through the opened TJs. This finding is consistent with reports from other researchers.[34,48]

The *in vivo* pharmacological efficacy showed good correlations with the improved cellular uptake and transport of insulin in the *in vitro* cell studies. The relative pharmacological availability of the orally administered Ins PLGA NPs and Ins TMC-PLGA NPs was significantly higher than that of insulin in solution, which was attributable to the protective effect and enhanced epithelial cell-penetrating ability of the nanoparticles in the GI tract. Furthermore, the pharmacological availability of the Ins TMC-PLGA NPs was 2 times greater than that of the Ins PLGA NPs (Table 2). The mucoadhesion property of the TMC-PLGA NPs partly accounted for the better absorption of insulin. After oral administration, the TMC-PLGA NPs soon attached to the mucus layer in the lower part of the small intestine and remained there for a relatively long time (Figure 6). The small intestine is regarded as a more favorable site for drug or nanoparticle absorption because of its larger surface area compared with that of the colon. Meanwhile, the TMC coating of the nanoparticles could facilitate mucus penetration, cellular internalization and the transport of insulin via the para-cellular route through TJ opening. All of the above effects of TMC-PLGA NPs overcome the multiple barriers to insulin absorption and improve the bioavailability of insulin, as reflected by the quick-onset, long-lasting hyperglycemia effect observed in diabetic rats (Figure 7). However, the BGLs in the diabetic rats did not return to their initial levels 12 h postdosing. This phenomenon has also been reported in other studies,[49,50] which might be attributable to the dual effects of insulin's hypoglycemic activity and prolonged starvation in diabetic rats.

Although a significantly enhanced hypoglycemia effect of orally delivered Ins TMC-PLGA NPs was observed after oral administration of Ins TMC-PLGA NPs, the BGL of diabetic rats did not return to the normal level (Supporting Information Table S2). The hypoglycemia effect failed to increase when the dose of insulin increased to 40 IU/kg (Supporting Information Table

DOI: 10.1021/acsami.5b03555
ACS Appl. Mater. Interfaces 2015, 7, 15430−15441

S3). The nanoparticles were probably aggregated in the GI tract, due to the higher concentration of nanoparticles administered. To improve further the absorption of insulin and to realize the stronger therapeutic effect after oral administration of insulin, the bioavailability of the large proportion of insulin released from nanoparticles should be improved. Encapsulation in our prepared TMC-PLGA NPs and enhancing the permeability of insulin molecules simultaneously might be a promising strategy.

5. CONCLUSIONS

TMC-PLGA NPs were prepared and characterized for oral insulin delivery. To a certain extent, TMC-PLGA NPs could protect insulin from enzymatic degradation in the GI tract. Compared with PLGA NPs, encapsulation in TMC-PLGA NPs could also significantly improve the mucus and epithelial cells penetration of insulin. Furthermore, mucoadhesive TMC-PLGA NPs could attach to the lower part of the small intestine after oral administration, prolonging the retention time at the absorption site. Therefore, TMC-PLGA NPs could overcome the multiple barriers to oral insulin absorption, and the pharmacological availability of insulin was significantly enhanced after oral administration in diabetic rats. These results suggested that the TMC-PLGA NPs developed in this study could potentially be employed for the oral delivery of therapeutic proteins.

■ ASSOCIATED CONTENT

Supporting Information

Characterizations of fluorescein or radioisotope-labeled nanoparticles, blood glucose values in diabetic rats and cytotoxicity of nanoparticles. The Supporting Information is available free of charge on the ACS Publications website at DOI: 10.1021/acsami.5b03555.

■ AUTHOR INFORMATION

Corresponding Author

*J. Wang. Tel.: +86-21-51980088. Fax: +86-21-5198 0087. E-mail: jxwang@fudan.edu.cn.

Notes

The authors declare no competing financial interest.

■ ACKNOWLEDGMENTS

We are thankful for financial support from the National Science and Technology Major Project (No. 2012ZX09304004).

■ REFERENCES

(1) Tahrani, A. A.; Bailey, C. J.; Del Prato, S.; Barnett, A. H. Management of Type 2 Diabetes: New and Future Developments in Treatment. *Lancet* **2011**, *378*, 182−197.

(2) Arbit, E. The Physiological Rationale for Oral Insulin Administration. *Diabetes Technol. Ther.* **2004**, *6*, 510−7.

(3) Sonaje, K.; Lin, K.; Wey, S.; Lin, C.; Yeh, T.; Nguyen, H.; Hsu, C.; Yen, T.; Juang, J.; Sung, H. Biodistribution, Pharmacodynamics and Pharmacokinetics of Insulin Analogues in a Rat Model: Oral Delivery Using pH-Responsive Nanoparticles vs. Subcutaneous Injection. *Biomaterials* **2010**, *31*, 6849−6858.

(4) Smart, A. L.; Gaisford, S.; Basit, A. W. Oral Peptide and Protein Delivery: Intestinal Obstacles and Commercial Prospects. *Expert Opin. Drug Delivery* **2014**, *11*, 1323−1335.

(5) Ensign, L. M.; Cone, R.; Hanes, J. Oral Drug Delivery with Polymeric Nanoparticles: The Gastrointestinal Mucus Barriers. *Adv. Drug Delivery Rev.* **2012**, *64*, 557−570.

(6) Lagarce, F.; Groo, A.; Saulnier, P.; Gimel, J.; Gravier, J.; Ailhas, C.; Benoit, J. Fate of Paclitaxel Lipid Nanocapsules in Intestinal Mucus in View of their Oral Delivery. *Int. J. Nanomed.* **2013**, 4291.

(7) Chen, M.; Sonaje, K.; Chen, K.; Sung, H. A Review of the Prospects for Polymeric Nanoparticle Platforms in Oral Insulin Delivery. *Biomaterials* **2011**, *32*, 9826−9838.

(8) Lee, E.; Lee, J.; Jon, S. A Novel Approach to Oral Delivery of Insulin by Conjugating with Low Molecular Weight Chitosan. *Bioconjugate Chem.* **2010**, *21*, 1720−1723.

(9) Gao, X.; Cao, Y.; Song, X.; Zhang, Z.; Zhuang, X.; He, C.; Chen, X. Biodegradable, pH-Responsive Carboxymethyl Cellulose/Poly(acrylic acid) Hydrogels for Oral Insulin Delivery. *Macromol. Biosci.* **2014**, *14*, 565−575.

(10) Déat-Lainé, E.; Hoffart, V.; Garrait, G.; Jarrige, J.; Cardot, J.; Subirade, M.; Beyssac, E. Efficacy of Mucoadhesive Hydrogel Microparticles of Whey Protein and Alginate for Oral Insulin Delivery. *Pharm. Res.* **2013**, *30*, 721−734.

(11) Maroni, A.; Zema, L.; Del Curto, M. D.; Foppoli, A.; Gazzaniga, A. Oral Colon Delivery of Insulin with the Aid of Functional Adjuvants. *Adv. Drug Delivery Rev.* **2012**, *64*, 540−556.

(12) Zhang, L.; Zhang, Z.; Li, N.; Wang, N.; Wang, Y.; Tang, S.; Xu, L.; Ren, Y. Synthesis and Evaluation of a Novel B-Cyclodextrin Derivative for Oral Insulin Delivery and Absorption. *Int. J. Biol. Macromol.* **2013**, *61*, 494−500.

(13) Shan, W.; Zhu, X.; Liu, M.; Li, L.; Zhong, J.; Sun, W.; Zhang, Z.; Huang, Y. Overcoming the Diffusion Barrier of Mucus and Absorption Barrier of Epithelium by Self-Assembled Nanoparticles for Oral Delivery of Insulin. *ACS Nano* **2015**, *9*, 2345−2356.

(14) Card, J. W.; Magnuson, B. A. A Review of the Efficacy and Safety of Nanoparticle-Based Oral Insulin Delivery Systems. *AJP: Gastrointestinal and Liver Physiology* **2011**, *301*, G956−G967.

(15) Yan, L.; Wang, H.; Jiang, Y.; Liu, J.; Wang, Z.; Yang, Y.; Huang, S.; Huang, Y. Cell-Penetrating Peptide-Modified PLGA Nanoparticles for Enhanced Nose-to-Brain Macromolecular Delivery. *Macromol. Res.* **2013**, *21*, 435−441.

(16) Wang, H.; Zhao, Y.; Wang, H.; Gong, J.; He, H.; Shin, M. C.; Yang, V. C.; Huang, Y. Low-Molecular-Weight Protamine-Modified PLGA Nanoparticles for Overcoming Drug-Resistant Breast Cancer. *J. Controlled Release* **2014**, *192*, 47−56.

(17) Zhang, L.; Han, L.; Qin, J.; Lu, W.; Wang, J. The Use of Borneol as an Enhancer for Targeting Aprotinin-Conjugated PEG-PLGA Nanoparticles to the Brain. *Pharm. Res.* **2013**, *30*, 2560−2572.

(18) Jain, S.; Rathi, V. V.; Jain, A. K.; Das, M.; Godugu, C. Folate-Decorated PLGA Nanoparticles as a Rationally Designed Vehicle for the Oral Delivery of Insulin. *Nanomedicine* **2012**, *7*, 1311−1337.

(19) Wu, Z. M.; Zhou, L.; Guo, X. D.; Jiang, W.; Ling, L.; Qian, Y.; Luo, K. Q.; Zhang, L. J. HP55-Coated Capsule Containing PLGA/RS Nanoparticles for Oral Delivery of Insulin. *Int. J. Pharm.* **2012**, *425*, 1−8.

(20) Reix, N.; Parat, A.; Seyfritz, E.; Van Der Werf, R.; Epure, V.; Ebel, N.; Danicher, L.; Marchioni, E.; Jeandidier, N.; Pinget, M.; Frère, Y.; Sigrist, S. *In Vitro* Uptake Evaluation in Caco-2 Cells and *In Vivo* Results in Diabetic Rats of Insulin-Loaded PLGA Nanoparticles. *Int. J. Pharm.* **2012**, *437*, 213−220.

(21) Yu, F.; Li, Y.; Liu, C. S.; Chen, Q.; Wang, G. H.; Guo, W.; Wu, X. E.; Li, D. H.; Wu, W. D.; Chen, X. D. Enteric-Coated Capsules Filled with Mono-Disperse Micro-Particles Containing PLGA-Lipid-PEG Nanoparticles for Oral Delivery of Insulin. *Int. J. Pharm.* **2015**, *484*, 181−191.

(22) Hosseininasab, S.; Pashaei-Asl, R.; Khandaghi, A. A.; Nasrabadi, H. T.; Nejati-Koshki, K.; Akbarzadeh, A.; Joo, S. W.; Hanifehpour, Y.; Davaran, S. Synthesis, Characterization, and *in Vitro* Studies of PLGA-PEG Nanoparticles for Oral Insulin Delivery. *Chem. Biol. Drug Des.* **2014**, *84*, 307−315.

(23) Chen, M.; Mi, F.; Liao, Z.; Hsiao, C.; Sonaje, K.; Chung, M.; Hsu, L.; Sung, H. Recent Advances in Chitosan-Based Nanoparticles for Oral Delivery of Macromolecules. *Adv. Drug Delivery Rev.* **2013**, *65*, 865−879.

(24) Kumar, M.; Pandey, R. S.; Patra, K. C.; Jain, S. K.; Soni, M. L.; Dangi, J. S.; Madan, J. Evaluation of Neuropeptide Loaded Trimethyl Chitosan Nanoparticles for Nose to Brain Delivery. *Int. J. Biol. Macromol.* **2013**, *61*, 189−195.

(25) Kotze, A. F.; Luessen, H. L.; de Leeuw, B. J.; de Boer, A. G.; Verhoef, J. C.; Junginger, H. E. Comparison of the Effect of Different

DOI: 10.1021/acsami.5b03555
ACS Appl. Mater. Interfaces 2015, 7, 15430−15441

Chitosan Salts and *N*-Trimethyl Chitosan Chloride on the Permeability of Intestinal Epithelial Cells (Caco-2). *J. Controlled Release* **1998**, *51*, 35−46.
(26) Sadeghi, A.; Dorkoosh, F.; Avadi, M.; Weinhold, M.; Bayat, A.; Delie, F.; Gurny, R.; Larijani, B.; Rafieetehrani, M.; Junginger, H. Permeation Enhancer Effect Of Chitosan And Chitosan Derivatives: Comparison of Formulations as Soluble Polymers and Nanoparticulate Systems on Insulin Absorption in Caco-2 Cells. *Eur. J. Pharm. Biopharm.* **2008**, *70*, 270−278.
(27) Jin, Y.; Song, Y.; Zhu, X.; Zhou, D.; Chen, C.; Zhang, Z.; Huang, Y. Goblet Cell-Targeting Nanoparticles for Oral Insulin Delivery and the Influence of Mucus On Insulin Transport. *Biomaterials* **2012**, *33*, 1573−1582.
(28) Mi, F.; Wu, Y.; Lin, Y.; Sonaje, K.; Ho, Y.; Chen, C.; Juang, J.; Sung, H. Oral Delivery of Peptide Drugs Using Nanoparticles Self-Assembled by Poly(γ-glutamic acid) and a Chitosan Derivative Functionalized by Trimethylation. *Bioconjugate Chem.* **2008**, *19*, 1248−1255.
(29) Zhang, J.; Zhu, X.; Jin, Y.; Shan, W.; Huang, Y. Mechanism Study of Cellular Uptake and Tight Junction Opening Mediated by Goblet Cell-Specific Trimethyl Chitosan Nanoparticles. *Mol. Pharmaceutics* **2014**, *11*, 1520−1532.
(30) Yin, L.; Ding, J.; He, C.; Cui, L.; Tang, C.; Yin, C. Drug Permeability and Mucoadhesion Properties of Thiolated Trimethyl Chitosan Nanoparticles in Oral Insulin Delivery. *Biomaterials* **2009**, *30*, 5691−5700.
(31) Cohen-Sela, E.; Chorny, M.; Koroukhov, N.; Danenberg, H. D.; Golomb, G. A New Double Emulsion Solvent Diffusion Technique for Encapsulating Hydrophilic Molecules in PLGA Nanoparticles. *J. Controlled Release* **2009**, *133*, 90−95.
(32) Li, X.; Guo, S.; Zhu, C.; Zhu, Q.; Gan, Y.; Rantanen, J.; Rahbek, U. L.; Hovgaard, L.; Yang, M. Intestinal Mucosa Permeability Following Oral Insulin Delivery Using Core Shell Corona Nanolipoparticles. *Biomaterials* **2013**, *34*, 9678−9687.
(33) Behrens, I.; Pena, A. I.; Alonso, M. J.; Kissel, T. Comparative Uptake Studies of Bioadhesive and Non-Bioadhesive Nanoparticles in Human Intestinal Cell Lines and Rats: The Effect of Mucus on Particle Adsorption and Transport. *Pharm. Res.* **2002**, *19*, 1185−1193.
(34) Lin, Y.; Sonaje, K.; Lin, K. M.; Juang, J.; Mi, F.; Yang, H.; Sung, H. Multi-Ion-Crosslinked Nanoparticles with pH-Responsive Characteristics for Oral Delivery of Protein Drugs. *J. Controlled Release* **2008**, *132*, 141−149.
(35) He, H.; Sheng, J.; David, A. E.; Kwon, Y. M.; Zhang, J.; Huang, Y.; Wang, J.; Yang, V. C. The Use of Low Molecular Weight Protamine Chemical Chimera to Enhance Monomeric Insulin Intestinal Absorption. *Biomaterials* **2013**, *34*, 7733−7743.
(36) Landry, F. B.; Bazile, D. V.; Spenlehauer, G.; Veillard, M.; Kreuter, J. Degradation of Poly(D,L-lactic acid) Nanoparticles Coated with Albumin in Model Digestive Fluids (USP XXII). *Biomaterials* **1996**, *17*, 715−723.
(37) Williams, D. F.; Mort, E. Enzyme-Accelerated Hydrolysis of Polyglycolic Acid. *J. Bioeng.* **1977**, *1*, 231−238.
(38) Fredenberg, S.; Wahlgren, M.; Reslow, M.; Axelsson, A. The Mechanisms of Drug Release in Poly(lactic-*co*-glycolic acid)-Based Drug Delivery Systems—a Review. *Int. J. Pharm.* **2011**, *415*, 34−52.
(39) Emami, J.; Hamishehkar, H.; Najafabadi, A. R.; Gilani, K.; Minaiyan, M.; Mahdavi, H.; Nokhodchi, A. A Novel Approach to Prepare Insulin-Loaded Poly(lactic-*co*-glycolic acid) Microcapsules and the Protein Stability Study. *J. Pharm. Sci.* **2009**, *98*, 1712−1731.
(40) He, C.; Yin, L.; Tang, C.; Yin, C. Size-Dependent Absorption Mechanism of Polymeric Nanoparticles for Oral Delivery of Protein Drugs. *Biomaterials* **2012**, *33*, 8569−8578.
(41) Chung, T.; Wu, S.; Yao, M.; Lu, C.; Lin, Y.; Hung, Y.; Mou, C.; Chen, Y.; Huang, D. The Effect of Surface Charge on the Uptake and Biological Function of Mesoporous Silica Nanoparticles in 3T3-L1 Cells and Human Mesenchymal Stem Cells. *Biomaterials* **2007**, *28*, 2959−2966.
(42) Chen, L.; Mccrate, J. M.; Lee, J. C.; Li, H. The Role of Surface Charge on the Uptake and Biocompatibility of Hydroxyapatite Nanoparticles with Osteoblast Cells. *Nanotechnology* **2011**, *22*, 105708.
(43) Yang, M.; Lai, S. K.; Wang, Y. Y.; Zhong, W.; Happe, C.; Zhang, M.; Fu, J.; Hanes, J. Biodegradable Nanoparticles Composed Entirely of Safe Materials that Rapidly Penetrate Human Mucus. *Angew. Chem., Int. Ed.* **2011**, *50*, 2597−600.
(44) Artursson, P.; Palm, K.; Luthman, K. Caco-2 Monolayers in Experimental and Theoretical Predictions of Drug Transport. *Adv. Drug Delivery Rev.* **2012**, *64*, 280−289.
(45) Smith, J.; Wood, E.; Dornish, M. Effect of Chitosan On Epithelial Cell Tight Junctions. *Pharm. Res.* **2004**, *21*, 43−49.
(46) Sonaje, K.; Lin, K.; Tseng, M. T.; Wey, S.; Su, F.; Chuang, E.; Hsu, C.; Chen, C.; Sung, H. Effects of Chitosan-Nanoparticle-Mediated Tight Junction Opening On the Oral Absorption of Endotoxins. *Biomaterials* **2011**, *32*, 8712−8721.
(47) Basson, M. D.; Emenaker, N. J.; Rashid, Z. Effects of Modulation of Tyrosine Phosphorylation On Brush Border Enzyme Activity in Human Caco-2 Intestinal Epithelial Cells. *Cell Tissue Res.* **1998**, *292*, 553−62.
(48) Vllasaliu, D.; Exposito-Harris, R.; Heras, A.; Casettari, L.; Garnett, M.; Illum, L.; Stolnik, S. Tight Junction Modulation by Chitosan Nanoparticles: Comparison with Chitosan Solution. *Int. J. Pharm.* **2010**, *400*, 183−193.
(49) Sonaje, K.; Lin, Y.; Juang, J.; Wey, S.; Chen, C.; Sung, H. In Vivo Evaluation of Safety and Efficacy of Self-Assembled Nanoparticles for Oral Insulin Delivery. *Biomaterials* **2009**, *30*, 2329−2339.
(50) Cui, F.; Shi, K.; Zhang, L.; Tao, A.; Kawashima, Y. Biodegradable Nanoparticles Loaded with Insulin-Phospholipid Complex for Oral Delivery: Preparation, *in Vitro* Characterization and *in Vivo* Evaluation. *J. Controlled Release* **2006**, *114*, 242−250.

DOI: 10.1021/acsami.5b03555
ACS Appl. Mater. Interfaces 2015, 7, 15430−15441